Projection effects in electron micrographs of three-dimensional fractal aggregates: theory and application to gas-evaporated specimens

1989 J. Phys.: Condens. Matter 1 2451

(http://iopscience.iop.org/0953-8984/1/14/001)

J. Phys.: Condens. Matter **1** (1989) 2451–2463. Printed in the UK

Projection effects in electron micrographs of three-dimensional fractal aggregates: theory and application to gas-evaporated specimens

T Farestam† and G A Niklasson‡

† Institute of Theoretical Physics, Chalmers University of Technology, S-412 96 Göteborg, Sweden

‡ Physics Department, Chalmers University of Technology, S-412 96 Göteborg, Sweden

Received 10 October 1988

Abstract. We analyse electron micrographs which show projections of three-dimensional fractal aggregates. Shadowing and finite size effects in the projection are treated by calculations for two model systems, namely a single aggregate and a connected aggregate. The calculations allow us to obtain the fractal dimension of the aggregates from the measured effective dimensions on the micrographs.

Aggregates of metal particles were produced by gas evaporation and studied by electron microscopy. We analysed the structure of the specimens by the connected-aggregate model. Fractal dimensions in the range 1.9 to 2.0 were found. This is in good agreement with the cluster–cluster aggregation model if the aggregating particles follow linear trajectories.

1. Introduction

The study of fractal structures in physics has recently attracted much interest (Mandelbrot 1983, Pietronero and Tosatti 1986). Fractal structures can be characterised by various experimental methods such as image analysis of electron micrographs (Forrest and Witten 1979, Chevalier *et al* 1985, Tence *et al* 1986) scattering of light, x-rays and neutrons (Teixeira 1986, Martin and Hurd 1987, Freltoft *et al* 1986), and adsorption measurements (Pfeifer and Avnir 1983, Avnir *et al* 1983, 1984, 1985). In this paper we consider the problem of obtaining the fractal dimension of a three-dimensional (3D) structure from the analysis of a projection of the structure onto a plane. This problem arises frequently in the study of large colloidal or gas-evaporated aggregates by electron microscopy. In order to establish the growth mechanisms of these aggregates it is of prime importance to have access to reliable methods of estimating the fractal dimension from electron micrographs.

In § 2 below we formulate a theoretical model for the projection of a fractal structure onto a plane. The model takes into account the finite correlation length as discussed by Tence *et al* (1986), but we also include the effect that all particles are not seen in the image because they are shadowing each other. Our model is applicable to the analysis of bright-field electron microscopy, while effects of shadowing do not enter when annular dark-field images (Chevalier *et al* 1985) are analysed, as noted by Tence *et al* (1986). We analyse the effects of shadowing and of cut-offs to the fractal structure for two model

0953-8984/89/142451 + 13 $02.50

structures, namely a single-aggregate model and a connected-aggregate model. Our computations enable us to correct the measured effective dimension of the projected image in order to obtain the real fractal dimension of the structure.

Subsequently in § 3 we apply our theoretical models to an experimental system, i.e. aggregates of gas-evaporated metal particles. The experimental effective dimensions are well accounted for by the connected-aggregate model. The fractal dimensions of the aggregates are found to be higher than in a previous study (Niklasson 1987), which did not correct the data for the effects of the projection. Our results are in good agreement with computer simulations using the cluster–cluster aggregation model with linear trajectories (Meakin 1984, Ball and Jullien 1984, Meakin 1985). Finally in § 4 we give some concluding remarks.

2. Theoretical models

In this section we study the effect on the measured effective dimension, D_{eff}, of the projection of a 3D fractal aggregate to a plane. The effective dimension can be obtained from the 2D image by measurement of the pair correlation function or by the 'nesting squares' method (Forrest and Witten 1979). From the measured D_{eff} we want to obtain information on the fractal dimension of the aggregate, D.

We consider two different models for a fractal structure. The structure is taken to be fractal for length scales between the size of the individual building blocks, a, and a certain correlation length, ξ. In the single-aggregate model we take the mass density of the structure to be zero for length scales larger than ξ. This model should be applicable to dilute dispersions of fractal aggregates. In the connected-aggregate model, on the other hand, the mass density of the structure is assumed to have a constant value for length scales larger than the correlation length. This model should be applicable to materials which display a crossover between fractal and non-fractal structure at the correlation length ξ.

For infinite ($\xi \to \infty$) fractal structures the projection of a 3D aggregate to 2D does not affect the value of the fractal dimension as long as D is less than two (Mandelbrot 1983). For $D > 2$ the projection has $D_{\text{eff}} = 2$, which is the dimensionality of the plane of projection. In reality ξ has a finite value and thus finite size effects will affect the measured D_{eff} of the projected image. We study the effects of a finite correlation length and of shadowing by calculations for a model structure.

2.1. Single-aggregate model

In order to calculate the projection effects we specify a model for a single fractal cluster. We study a continuous representation of a 3D spherically symmetric fractal aggregate with total mass M and correlation length ξ. The mass density $\rho(r)$ is taken to be

$$\begin{aligned} \rho(r) &= (MD/4\pi\xi^D)r^{D-3} \qquad r < \xi \\ \rho(r) &= 0 \qquad\qquad\qquad\qquad r > \xi. \end{aligned} \tag{1}$$

The mass can be written as $M = Nm_{\text{p}}$, where $N = (\xi/a)^D$ is the number of particles and

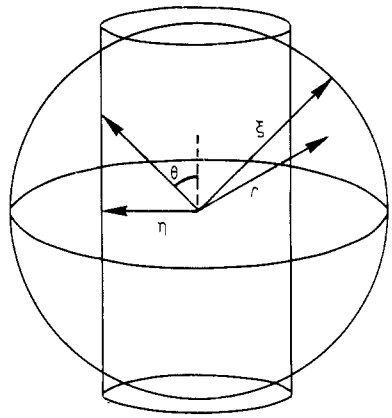

Figure 1. Geometry for projection of a spherically symmetric object onto the η-plane. The cylinder used for the calculation in (2) is also shown.

m_p is the mass of a single particle. The geometry is illustrated in figure 1. The radial coordinate in a coordinate system centred on the aggregate is denoted by r, while η is the radial coordinate in the plane of projection. The angle θ is defined by the relation $\sin\theta = \eta/r$. We now normalise the coordinate in the plane with respect to the correlation length and introduce the notation $q = \eta/\xi$.

First we calculate the effective dimension for the case when shadowing is neglected, and only the finite size of the aggregate is taken into account. Later we will also consider effects of shadowing. In what follows we put $m_p = 1$, i.e. we measure the mass in number of particles. The first step of the calculation is to consider a cylinder of radius η, whose axis goes through the centre of the aggregate (figure 1). The number of particles within radius η, N_0, is then given by (Tence *et al* 1986)

$$N_0(\eta) = 4\pi \int_0^{\eta} r^2 \rho(r)\, dr + 4\pi \int_0^{\xi} (1 - \cos\theta) r^2 \rho(r)\, dr. \tag{2}$$

In terms of the normalised coordinates this is equivalent to

$$N_0(q) = (\xi/a)^D q^D (1 + Df(q)) \tag{3}$$

where

$$f(q) = \int_q^1 (1 - \sqrt{1 - z^2})\, dz/z^{D+1}.$$

Equation (3) now gives the number of particles projected onto the plane within a distance q of the origin. Figure 2 shows a log–log plot of N_0/N as a function of q for different values of D. The effective dimension of the projection is defined by $N_0(q) = kq^{D_{\text{eff}}}$, where k is a constant. It is immediately seen that D_{eff} is given by the slopes of the curves in figure 2. In figure 3 we show the quantity $(D_{\text{eff}} - D)$ as a function of D for several values of q. It is seen that the difference $(D_{\text{eff}} - D)$ is small for fractal dimensions close to unity and for small q, but it increases quickly as we increase D and q.

When projecting a fractal structure onto a plane, some of the particles in the structure must necessarily shadow each other. We now include in our model the probability that

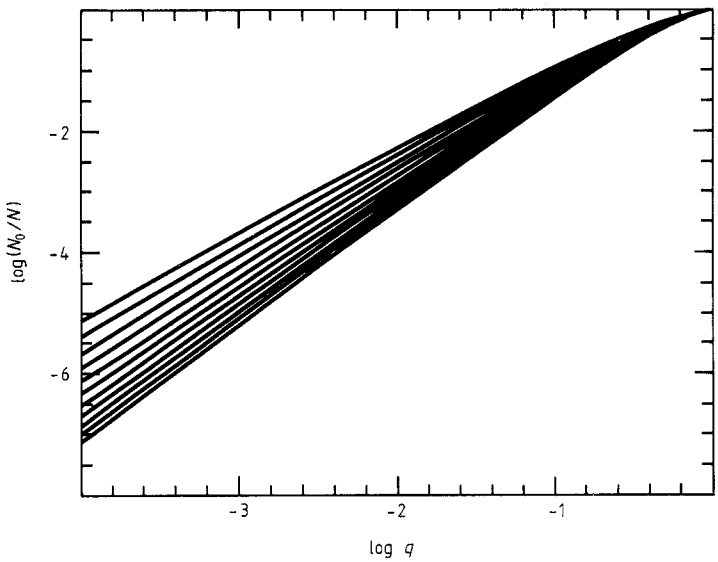

Figure 2. Log–log plot of normalised number of particles N_0/N as a function of the normalised coordinate q ($=\eta/\xi$, cf figure 1) in the plane of projection. Curves denote results for fractal dimensions between 1.5 (top) and 2.5 (bottom). The difference in D between consecutive curves is 0.1.

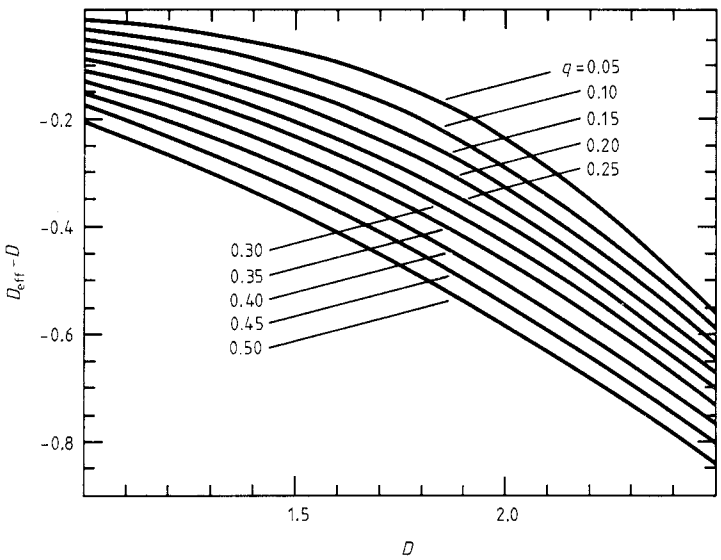

Figure 3. Values of $D_{eff} - D$, calculated by the single-aggregate model, as a function of the fractal dimension D for various values of the coordinate in the plane q. Effects of shadowing are not taken into account.

particles shadow each other. The basic idea can be illustrated by a simple example. Take 100 cubes, put them on top of one another and assume that the probability for a cube to be occupied is 0.01 and for it to be empty is 0.99. If the stack of cubes is projected onto a plane the probability is $1 - 0.99^{100} = 0.63$ that we see an occupied square in the plane

of projection. Generally we consider a large number, n, of cubes in a stack and take the probability for a cube to be occupied to be equal to n_0/n. The probability to obtain an occupied square in the projection then becomes, in the limit of large n

$$\lim_{n\to\infty}[1-(1-n_0/n)^n] = 1-\exp(-n_0).$$

Shadowing effects in the projection of a fractal aggregate are completely analogous, and we obtain the area fraction of occupied sites, $\sigma(q)$, from the relation

$$\sigma(q) = 1-\exp(-\mu(q)). \tag{4}$$

Here $\mu(q)$ is the average number of projected particles at distance q. This can be evaluated from the projected number of particles within distance q $N_0(q)$ in (3). We obtain

$$\mu(q) = \frac{1}{2\pi q}\left(\frac{\pi a^2}{\xi^2}\right)\frac{\mathrm{d}}{\mathrm{d}q}N_0(q). \tag{5}$$

In order to make contact with experiments we need to evaluate the number of observed particles within a distance q in the plane of projection. This surface coverage $N_1(q)$ is given by

$$N_1(q) = (\xi^2/\pi a^2)\int_0^q \sigma(q')\,2\pi q'\,\mathrm{d}q' \tag{6}$$

where $\sigma(q')$ is given in (4). A closed expression for $N_1(q)$ is now easily obtained from (3)–(6). The final expression becomes

$$N_1(q) = 2\left(\frac{\xi}{a}\right)^2\int_0^q\left\{1-\exp\left[-\frac{D}{2}\left(\frac{\xi}{a}\right)^{D-2}\right.\right.$$
$$\left.\left.\times\, q^{D-2}\left(1+Df(q')+q'\frac{\mathrm{d}}{\mathrm{d}q'}f(q')\right)\right]\right\}q'\,\mathrm{d}q'. \tag{7}$$

The effective dimension D_{eff} can be obtained from (7) by use of the identity $N_1(q) = kq^{D_{\mathrm{eff}}}$. Figure 4 shows $(D_{\mathrm{eff}}-D)$ as a function of D for this case. It is seen that the correction $(D_{\mathrm{eff}}-D)$ is smaller when D_{eff} is obtained from (7) than when it is obtained from (3). Thus the corrections become smaller when shadowing is included.

In figure 5 we show D_{eff} as a function of the coordinate q for several values of the fractal dimension D. This plot is very convenient for comparison with experiments. The fractal dimension of the sample can then be found by comparing an experimental $D_{\mathrm{eff}}(q)$ with the curves in figure 5.

2.2. *The connected-aggregate model*

In many cases fractal aggregates are connected into a network. This structure arises for example in gas-evaporated aggregates and can be described as a fractal structure which is embedded in a non-fractal surrounding. Therefore we now use a model with the mass density constant and equal to the mean density ρ_s when $r > \xi$, namely

$$\begin{aligned}\rho(r) &= (MD/4\pi\xi^D)r^{D-3} && r<\xi\\ \rho(r) &= \rho_s && r>\xi.\end{aligned} \tag{8}$$

We take a cube of side length 2ξ, and inside it we place a sphere of radius ξ containing

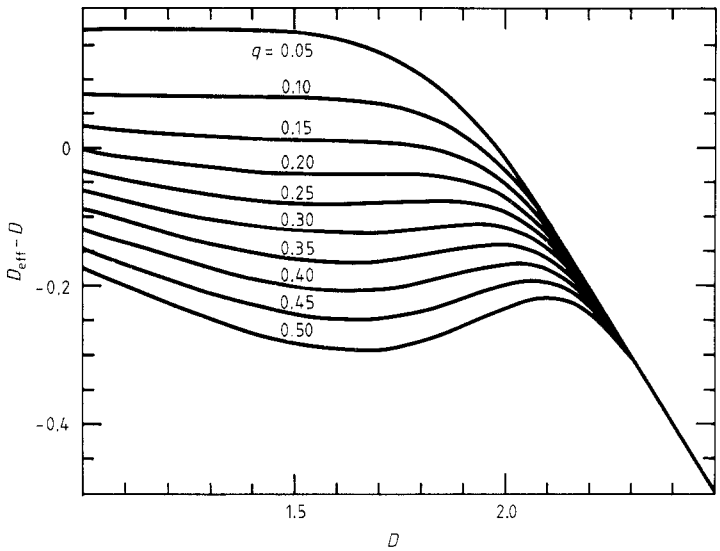

Figure 4. Values of $D_{eff} - D$, calculated by the single-aggregate model, as a function of the fractal dimension D and distance q. Shadowing effects are included and $\xi/a = 100$.

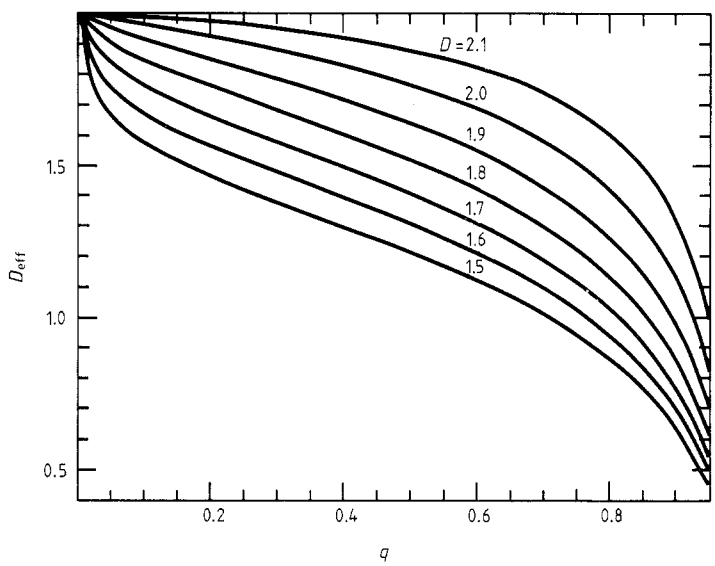

Figure 5. Effective dimension D_{eff} in the single-aggregate model as a function of distance q for various values of the fractal dimension D. ($\xi/a = 100$.)

a fractal aggregate. The density in the volume between the sphere and the cube is $\rho(r) = \rho_s$ according to (8).

We now project the particles in this volume onto a plane. The average number of projected particles within distance q from the origin is then given by

$$N_r(q) = 2\rho_s(\xi/a)^3[\pi q^2 + 2\pi(1 - q^2)^{3/2}/3 - 2\pi/3]. \tag{9}$$

When considering the connected-aggregate model we have two contributions to the

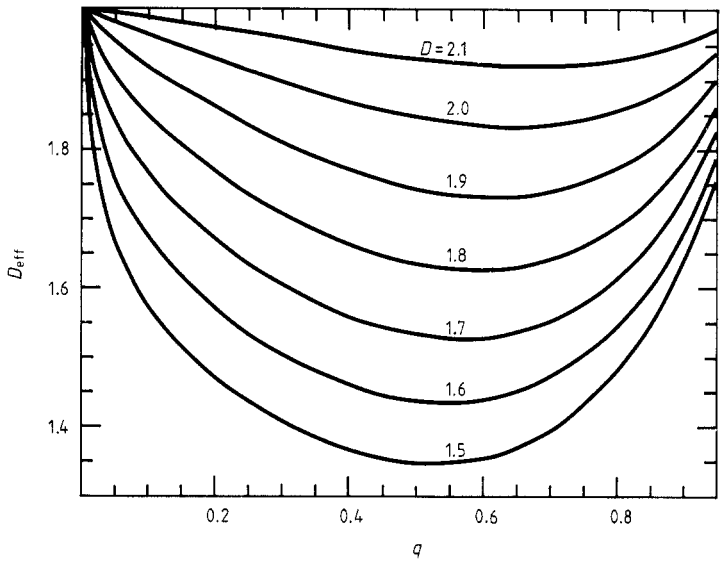

Figure 6. Effective dimension D_{eff} in the connected-aggregate model as a function of distance q for various values of the fractal dimension D. ($\xi/a = 100$.)

number of projected particles, namely from the fractal aggregate in the sphere (3) and from the volume between the sphere and the cube (9). The calculations for this model are completely analogous to those for the single-aggregate model in § 2.1. The quantity $\mu(q)$ in (5) must be replaced by the sum of the two contributions discussed above and is given by

$$\mu_{\text{tot}}(q) = \mu_r(q) + \mu(q).$$

Here $\mu(q)$ is given by (5) as before. In addition $\mu_r(q)$ is obtained from (5) when we replace $N_0(q)$ by $N_r(q)$ from (9). The surface coverage for the connected-aggregate model, $N_2(q)$, is given again by (4) and (6) if $\mu_{\text{tot}}(q)$ is used instead of $\mu(q)$ in (4). The final expressions for $\mu_{\text{tot}}(q)$ and $N_2(q)$ now become

$$\mu_{\text{tot}}(q) = (\xi/a)^{D-2}[(Dq^{D-2}/2)\,(1 + Df(q) + q(\mathrm{d}/\mathrm{d}q)f(q)) + \tfrac{3}{2}(1 - \sqrt{1-q^2})] \qquad (10)$$

and

$$N_2(q) = 2(\xi/a)^2 \int_0^q [1 - \exp(-\mu_{\text{tot}}(q'))]q'\,\mathrm{d}q'. \qquad (11)$$

The effective dimension can be obtained from (11) in the same way as for the single-aggregate model. Physically we can place some requirements on the function $D_{\text{eff}}(q)$. It is easy to show that D_{eff} must approach two as q goes towards zero and unity. This is so because the structure becomes non-fractal inside a single particle ($r < a$) and outside the correlation length ($r > \xi$). Figure 6 shows D_{eff} as a function of q for the connected-aggregate model. It is seen that $D_{\text{eff}}(q)$ satisfies the physical limits we mentioned above. A shortcoming of the model is that it does not take into account all finite size effects. We do not in reality deal with a mass density as in the model but instead we have a number of discrete particles. Thus it is obvious that the model does not work well when η is of the order a. Also the form of $\rho(r)$ for $r > \xi$ may be different in different physical

situations. For example $\rho(r)$ may have oscillations superimposed on the constant value ρ_s. Hence our model must be regarded as an approximation for large r. From figures 5 and 6 it is seen that the connected-aggregate and single-aggregate models give very similar results for small values of q. Only when $q > 0.4$ to 0.5 do considerable differences appear. In order to distinguish between the models, the effective dimension has to be measured over the whole range of q between zero and unity. On the other hand, if D_{eff} is measured at low q only, the precise form of the outer cut-off to the fractal structure does not enter in the estimation of the fractal dimension D. These considerations are important when comparing with experiments as we proceed to do in the next section.

3. Experimental results

In this section we compare the results of our calculations to experiments on a real system, namely gas-evaporated aggregates of metal particles. The agreement is found to be satisfactory, which points to the usefulness of our method for the determination of the fractal dimension. The structural analysis is of interest in order to understand the growth of the aggregates.

Gas evaporation takes place from an evaporation source, usually a tungsten coil, in a few torr of an inert gas such as helium, argon or nitrogen. Sometimes a small addition of oxygen is used in order to grow oxide coatings on the metal particles during the evaporation. The particles grow and form extended aggregates in the gas phase. This process has been extensively studied; for a review see, for example, Granqvist and Buhrman (1976). The metal atoms which escape from the evaporation source rapidly lose their energy by collisions with the gas atoms. This leads to a local supersaturation of metal and to homogeneous nucleation of metal clusters. Subsequently the metal nuclei grow by coalescence to form larger particles; probably this growth takes place in a region close to the evaporation source (Granqvist and Buhrman 1976). The vapour temperature must be quite high, i.e. in excess of 200–400 °C, for coalescence to take place (Kaito and Shiojiri 1982, Kaito 1985). At lower vapour temperatures the particles instead stick to one another when they collide eventually forming large porous aggregates (Forrest and Witten 1979). The aggregates are transported by gas convection in the evaporation chamber and can be collected on a substrate. The deposits are soot-like loosely packed powders having a volume fraction of metal usually of the order of one per cent. The average thickness of the deposits can be appreciable; typically it is around 10 μm or even larger, as determined by optical microscopy. Clearly the gas-evaporated metal deposits form a 3D porous coating on the substrate.

We have examined a number of gas-evaporated aggregates, deposited onto carbon-covered copper grids, by electron microscopy. The evaporation and preparation conditions are listed in table 1. Most of the samples were studied in the as-deposited state. One sample of Ni particles was partially oxidised by heating to 400 °C in air prior to electron microscopy. Some samples of Al particles were stored in a container for about 10 years. The powder was then mixed with ethanol and aggregates were collected on copper grids.

Figure 7 shows an electron micrograph of an aggregate of ultrafine Al particles evaporated in 3 Torr helium with a small addition of oxygen. It is seen that the metal particles form an aggregated structure consisting of clusters and chains of particles. The micrograph is a 2D image of the 3D aggregate.

Table 1. Preparation conditions, correlation length divided by particle radius, ξ/a, and fractal dimensions D for metal particle aggregates.

Metal	Evaporated in	ξ/a	D
Al	3 Torr He + O_2	~90	1.91
Al	1.5 Torr Ar + O_2	~90	1.97
Al	1.5 Torr Ar + O_2	~60	2.02
Co	1 Torr He	~40	1.95
Cr	2.5 Torr Ar + 0.1 Torr air	~60	1.95
Fe	2 Torr Ar	~15	1.90
Ni	2 Torr Ar	~90	1.91
Ni	2 Torr Ar and oxidised at 400 °C in air	~10	1.95

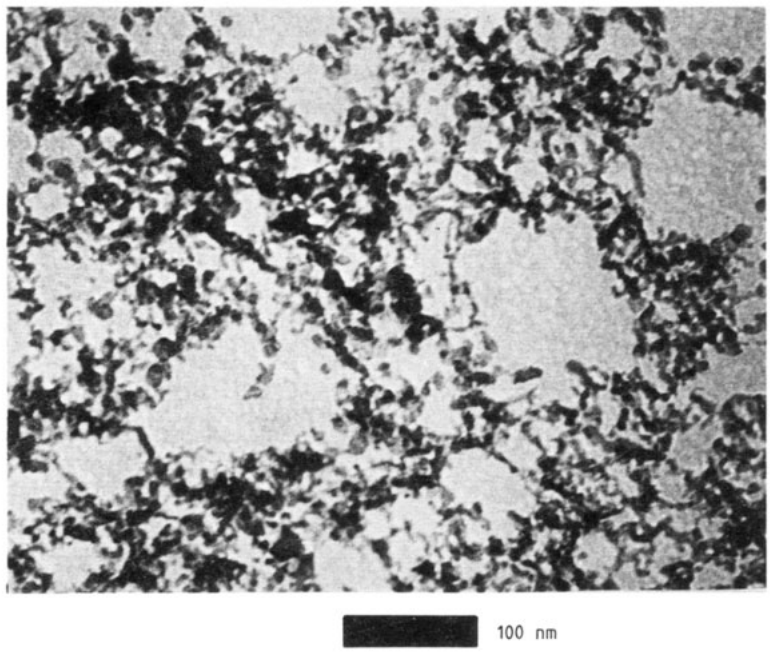

Figure 7. Electron micrograph of Al aggregates evaporated in 3 Torr He with a small addition of oxygen. The bar in the figure denotes 100 nm.

In order to determine whether the aggregates are fractal and to find the fractal dimension from the micrographs we first evaluated the pair correlation function of the particles. We measured the centre-to-centre distances between all particles within a certain area on the micrograph. The number of particles, N, within a distance η from a starting point was then obtained and averaged by taking each particle in turn as the starting point. This averaging was necessary in order to get good statistics. The pair correlation function can now be obtained from

$$g_2(\eta) = N(\eta)/\pi\eta^2\rho_s \tag{12}$$

where ρ_s is the average particle density.

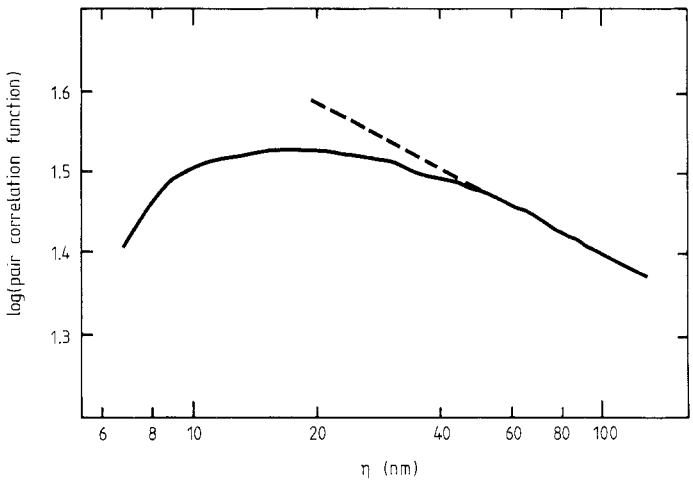

Figure 8. Log–log plot of the pair correlation function (in arbitrary units) as a function of the distance for the Al particles shown in figure 7. The broken line indicates a linear fit to $g_2(\eta) \sim \eta^{D-2}$, with $D = 1.75$.

Figure 8 shows the logarithm of $g_2(\eta)$ for the Al particles depicted in figure 7. The pair correlation function reaches a plateau at a distance of a few times the diameter of a single particle and then starts to decrease. This decrease signifies an unambiguous departure from a random arrangement of particles. At larger η the curve can be approximated by a straight line, as shown in the figure. A fit to the relation

$$g_2(\eta) \sim \eta^{D-2} \tag{13}$$

at large η gives $D = 1.75$.

Now we want to ascertain whether the effects of projecting a 3D fractal structure onto a 2D micrograph are present in the data. Such effects would lead to a corrected value for the fractal dimension, as discussed in § 2. To this end we evaluate the effective dimensionality defined in § 2 from the relation

$$D_{\text{eff}}(\eta) = 2 + \mathrm{d}(\log g_2(\eta))/\mathrm{d}(\log \eta). \tag{14}$$

It is seen that $D_{\text{eff}}(\eta) - 2$ is just the slope of the log–log plot of $g_2(\eta)$ at distance η. $D_{\text{eff}}(\eta)$ was calculated numerically from the experimental data. Figure 9 shows the results for the Al particles in figure 7. Here we normalised η by the correlation length, ξ, which was estimated from the average cluster size on the micrograph. It is seen that the effective dimension decreases at small q and reaches a minimum at $q \sim 0.6$. This behaviour can be described by the connected-aggregate model, figure 5, but is not in line with the single-aggregate model. Figure 9 shows that our experimental data are in satisfactory agreement with calculations for the connected-aggregate model with $D = 1.91$. At short distances the effective dimension seems to be somewhat higher than expected from the calculations. This effect was seen in all our samples and is probably due to the size of the individual particles and the width of the size distribution of individual particles, which were not taken into account in the calculations. The connected-aggregate model gave a better fit to our experimental data than the single-aggregate model for all our samples of gas-evaporated particles.

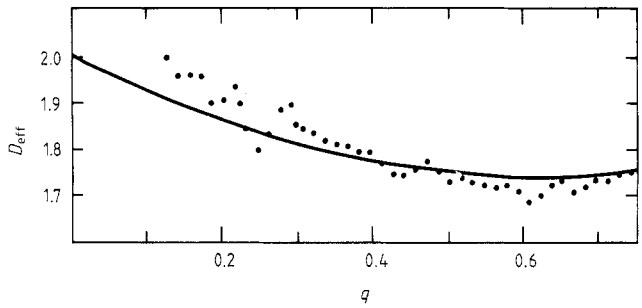

Figure 9. Effective dimension as a function of distance on the micrograph, q, for the Al particles shown in figure 7. Dots denote experimental data and the full curve shows a calculation by the connected-aggregate model with $D = 1.91$.

This kind of analysis was performed for the samples listed in table 1. The results were obtained from the analysis of one micrograph of each sample. The corrected value of the fractal dimension was determined by comparing the plots of $D_{\text{eff}}(q)$ against normalised distance with our calculations. The corrections always increased the value of D, as expected. The accuracy by which D can be determined depends on the noise in the experimental data; the uncertainty in D is usually ± 0.03 to 0.04. The values of the fractal dimension listed in table 1 fall, with two exceptions, in the range 1.90 to 1.95. The exceptions are the samples which had been stored for a long time before examination. However, we feel that the differences between the fractal dimensions are too small to permit any conclusions to be drawn from this. It is interesting to note that the kind of evaporated metal and the range of evaporation conditions explored in this paper seem to have very little influence on the fractal dimension. It should, however, be noted that strong dipolar interactions between the particles lead to a considerably lower fractal dimension of the aggregates. Such effects have recently been observed in aggregates composed of ferromagnetic Co particles (Niklasson *et al* 1988).

We now discuss the growth mechanisms of gas-evaporated aggregates. Situations where large aggregates are formed from smaller aggregates and single particles can be treated by cluster–cluster aggregation models (Meakin 1983, Kolb *et al* 1983). Computer simulations show that 3D cluster–cluster aggregates have fractal dimensions of 1.75–1.8 for the case of random-walk trajectories (Meakin 1984, Jullien *et al* 1984b). For linear trajectories the fractal dimension is somewhat higher. Off-lattice computer simulations give values of D in the range 1.87–2.0 (Meakin 1984, Ball and Jullien 1984, Meakin 1985). It has also been found that effects of structural readjustments (Meakin and Jullien 1985) and fragmentation (Kolb 1986) can increase the fractal dimension of cluster–cluster aggregates noticeably.

Our experimental fractal dimensions are in good agreement with the cluster–cluster aggregation model with linear trajectories. Linear trajectories are also physically reasonable in gas evaporation. At a gas pressure of 1 Torr the mean free path of aggregates moving in the gas can be estimated to be 50 to 100 μm. This is much larger than a single particle and about 100 times larger than a typical aggregate. Random-walk trajectories with mean free paths much larger than typical aggregate sizes give fractal dimensions very similar to the case of linear trajectories (Jullien *et al* 1984a).

To sum up, aggregation of metal particles in a low pressure gas can be described by the cluster–cluster model with linear trajectories. On the other hand, in colloidal

aggregation (Weitz and Oliveria 1984, Weitz *et al* 1985) the mean free paths are very short leading to random-walk trajectories and lower fractal dimensions.

4. Conclusions

In this paper we have addressed the problem of determining fractal dimensions from electron micrographs, which show a projection of the structure onto a plane. We formulated two models for the calculations of the structural characteristics in the projected image. The single-aggregate model should be applicable to a dilute dispersion of fractal aggregates, while the connected-aggregate model should be valid for fractal aggregates forming a percolating network. We have analysed the structure of aggregates of metal particles produced by gas evaporation by the above-mentioned models. Our experimental effective dimensions are in good agreement with calculations by the connected-aggregate model. This means that we can use the model to obtain the fractal dimension of the aggregate from the measured effective dimensions. The fractal dimension gives information on the growth mechanisms of the aggregates.

Aggregates of metal particles produced by gas evaporation were shown to have fractal dimensions in the range 1.9–2.0. These values are close to the predictions of cluster–cluster aggregation models with linear trajectories. The fractal dimension is fairly insensitive to the metal used and the evaporation conditions for systems where dipolar interactions between the particles can be neglected. We can now distinguish at least three different kinds of cluster–cluster aggregation. Aggregation in the gas phase with linear trajectories gives $D \sim 1.9$–2.0, while colloidal aggregation with Brownian trajectories leads to $D \sim 1.75$–1.8 (Weitz and Oliveria 1984, Weitz *et al* 1985). Finally aggregation of ferromagnetic particles leads to still lower fractal dimensions, namely $D \sim 1.4$–1.6 (Niklasson *et al* 1988).

Acknowledgments

This work was supported by grants from the Swedish Natural Science Research Council and the National Swedish Board for Technical Development. We appreciate valuable discussions with Dr P Apell and Dr C G Granqvist, as well as the communication of unpublished micrographs by Dr C G Granqvist. We thank Dr S Yatsuya for valuable assistance.

References

Avnir D, Farin D and Pfeifer P 1983 *J. Chem. Phys.* **79** 3566
—— 1984 *Nature* **308** 261
—— 1985 *J. Colloid Interface Sci.* **103** 112
Ball R C and Jullien R 1984 *J. Phys. Lett.* **45** L1031
Chevalier J-P, Colliex C and Tence M 1985 *J. Microsc. Scpectrosc. Electron.* **10** 417
Forrest S R and Witten Jr T A 1979 *J. Phys. A: Math. Gen.* **12** L109
Freltoft T, Kjems J K and Sinha S K 1986 *Phys. Rev.* B **33** 269
Granqvist C G and Buhrman R A 1976 *J. Appl. Phys.* **47** 2200
Jullien R, Kolb M and Botet R 1984a *Kinetics of Aggregation and Gelation* ed. F Family and D P Landau (Amsterdam: North-Holland) p 101
—— 1984b *J. Physique Lett.* **45** L211

Kaito C 1985 *Japan. J. Appl. Phys.* **24** 261
Kaito C and Shiojiri M 1982 *Japan. J. Appl. Phys.* **21** 1404
Kolb M 1986 *J. Phys. A: Math. Gen.* **19** L263
Kolb M, Botet R and Jullien R 1983 *Phys. Rev. Lett.* **51** 1123
Mandelbrot B B 1983 *The Fractal Geometry of Nature* (New York: W H Freeman)
Martin J E and Hurd A J 1987 *J. Appl. Crystallogr.* **20** 61
Meakin P 1983 *Phys. Rev. Lett.* **51** 1119
—— 1984 *Phys. Rev.* A **29** 997
—— 1985 *Phys. Lett.* **107A** 269
Meakin P and Jullien R 1985 *J. Physique* **46** 1543
Niklasson G A 1987 *J. Appl. Phys.* **62** 258
Niklasson G A, Torebring A, Larsson C, Granqvist C G and Farestam T 1988 *Phys. Rev. Lett.* **60** 1735
Pfeifer P and Avnir D 1983 *J. Chem. Phys.* **79** 3558
Pietronero L and Tosatti E eds. 1986 *Fractals in Physics* (Amsterdam: North-Holland)
Teixeira J 1986 in *On Growth and Form* ed. H E Stanley and N Ostrowsky (Dordrecht: Nijhoff) p 145
Tence M, Chevalier J P and Jullien R 1986 *J. Physique* **47** 1989
Weitz D A and Oliveria M 1984 *Phys. Rev. Lett.* **52** 1433
Weitz D A, Lin M Y and Sandroff C J 1985 *Surf. Sci.* **158** 147